Prediction of Boundary-Layer Flow Separation in V/STOL Engine Inlets

D.C. Chou,* R.W. Luidens,† and N.O. Stockman‡

NASA Lewis Research Center, Cleveland, Ohio

The paper provides a theoretical description of the development of the boundary layer on the lip and diffuser surface of a subsonic inlet at arbitrary operating conditions of mass flow rate, freestream velocity, and incident angle. Both laminar separation on the lip and turbulent separation in the diffuser are discussed. The agreement of the theoretical results with model experimental data illustrates the capability of the theory to predict separation location. The effects of throat Mach number, inlet size, and surface roughness on boundary-layer development and separation are illustrated.

Nomenclature

C_f = local skin friction coefficient (ratio of wall shear stress to dynamic pressure at edge of boundary layer)
D_e = diffuser exit diameter, cm
D_h = highlight diameter
D_{max} = maximum diameter
D_t = throat diameter
H = shape factor, ratio of boundary-layer displacement to momentum thickness
L = total length of inlet
L_e = length of centerbody
M = local Mach number
M_T = average one-dimensional throat Mach number based on inlet weight flow rate and geometric throat area
M_0 = freestream Mach number
$q^2/2$ = kinetic energy turbulence
R = Reynolds number
R_{ij} = Reynolds stress tensor
S = surface distance from inlet highlight
u/U_e = ratio of velocity in the boundary layer to velocity at the edge of the boundary layer
y = distance in the boundary layer normal to the inlet surface, cm
α = inlet incidence angle, deg
δ = boundary-layer thickness, cm
δ_k = kinematic displacement thickness
ϵ_m = eddy viscosity
ν = kinematic viscosity
θ = momentum thickness

Introduction

MANY proposed advanced aircraft, whether CTOL, STOL, or VTOL, require propulsion system inlets to operate over wide ranges of flight speed, incidence angle, and inlet throat Mach numbers (weight flow rates). A major design criterion for these types of inlets is that internal flow separation be avoided, particularly separation of the type that can cause unacceptable total pressure loss and distortion. This requirement can be quite severe for a fixed-geometry axisymmetric inlet. Therefore, considerable research and development effort is required for the design of such inlets.

The principal tool in inlet design has been wind-tunnel experiments with scale-model inlets. Wind-tunnel testing is both time-consuming and expensive. Furthermore, applying scale-model data to the design of full scale inlets may result in unnecessarily conservative designs. For these reasons a reliable theoretical method of predicting internal flow separation is desirable.

The NASA Lewis Research Center is currently in the process of developing such a method. It consists of a series of computer programs that calculate the potential and viscous flow, including separation prediction, in arbitrary inlets. Recent status reports on these programs are given in Refs. 1 and 2.

These programs were used to conduct a thorough investigation of the boundary-layer development on the lip and diffuser surface of an inlet designed for the Quiet Clean Short Haul Experimental Engine (QCSEE). The present paper presents some results from that investigation

Included are comparisons of theoretical with experimental separation bounds; some effects of varying the inlet operating conditions on the boundary-layer behavior; and a discussion of both lip and diffuser separation, and the stability of diffuser separation. The boundary-layer development is illustrated in detail for a typical set of operating conditions. Finally, the effects of surface roughness and of model scale (up to full size) are discussed.

Experimental Background

The inlet geometry chosen for the present study is shown in Fig. 1. Pertinent geometric parameters and terminology are indicated on the figure. Because of the great importance of efficient inlet flow on both engine performance and noise radiation suppression for advanced subsonic short-haul (STOL) aircraft, studies were initiated at the Lewis Research Center to investigate important flow parameters associated with several inlet geometries under the QCSEE project. One of the top candidates of the design is the so-called GE-2 inlet, which is chosen here, which has the geometric parameters listed in Table 1. Details of this design may be found in Ref. 3.

Tests for this and other inlets are performed in the Lewis Research Center 9 × 15 ft low-speed wind tunnel. A vacuum system was used in place of a fan or compressor to induce inlet flow. Inlet airflow is remotely varied using two butterfly

Presented as Paper 77-144 at the AIAA 15th Aerospace Sciences Meeting, Los Angeles, Calif., Jan 24-26, 1977; submitted March 24, 1977; revision received April 10, 1978.

Index categories: Aerodynamics; Airbreathing Propulsion.

*Present position, Division of Energy Engineering, the University of Iowa, Iowa City, Iowa. Member AIAA.

†Chief, Low Speed Aerodynamics Branch. Member AIAA.

‡Aerospace Engineer, Low Speed Aerodynamics Branch. Member AIAA.

Table 1 Inlet geometry parameters[a]

Inlet designation	Inlet area contraction ratio, $(D_h/D_{max.})^2$	External forebody $\frac{D_h}{D_{max}}$	Bluntness parameter, NB	$\frac{L_c}{D_e}$	Center body contour exponent for superellipse	$\frac{L}{D_e}$	Overall $\frac{D_{max}}{D_e}$
2A	1.46	0.905	0.0185	0.75	2.0	1	1.111

[a] D_h = highlight diameter, D_t = throat diameter, D_{max} = maximum diameter, D_e = exit diameter, L = total length of the inlet, and L_c = length of the center body.

valves arranged to give both coarse and fine adjustment. Inlet incidence angle is also remotely varied by mounting the test apparatus on a turntable. A swivel joint, containing a low-leakage pressure seal, provided 360 – deg rotation capability. Detailed discussion about the testing apparatus, procedure, and results may be found in the report by Miller et al.[4]

In order to compare the present analytical results with the existing experiment data, the input data based on the experimental operating conditions are given as follows. Two freestream Mach numbers of 0.12 and 0.18, respectively, representing some typical V/STOL aircraft operating conditions, are used in the calculation. For each set of freestream conditions, three representative average throat Mach numbers of 0.79, 0.6, and 0.3, which correspond to high, medium, and low inlet airflow situations, respectively, are chosen in the calculations to show the effect of airflow on the boundary-layer growth and the separation location (if any).

The experimental separation bounds, taken from Ref. 4, are shown in Fig. 2 on a plot of incidence angle α versus average throat Mach number. These data were obtained by setting the freestream Mach number and the throat Mach number (mass flow rate) and then increasing the inlet incidence angle to the point of observed lip separation. The angles used to generate the separation bounds shown on the figure are the angles just before the flow separates. The separation bounds appeared as bands rather than lines because of scatter in the data.

As illustrated in Fig. 3, if the incidence angle is increased just beyond the separation bound, separation occurs and the throat Mach number drops. This dropping of weight flow is observed experimentally at all throat Mach numbers and is illustrated on Fig. 3 for the lower throat Mach number range.

Calculation Procedure

The complete compressible viscous flowfield around the V/STOL engine axisymmetric inlet at an incidence angle is obtained by the NASA Lewis Inlet Computer Program. The computation is carried out by four steps. The first program, SCIRCL,[5] establishes the coordinates and point spacing on the inlet surfaces. The Douglas axisymmetric incompressible potential flow program,[6] called EOD here, is employed to give three basic solutions, which then can be combined by the third program called COMBYN, to obtain the potential solution for any combination of freestream velocity, inlet incidence angle, and mass flow rate through the inlet. The COMBYN program also corrects the incompressible potential flow solution by introducing the compressibility effects into the calculation. The compressibility effects are introduced by the Lieblein-Stockman procedure, which is fully described in Ref. 7.

The surface Mach number distribution, or the corresponding surface pressure distribution, can now be used as input to the VISCUS, which calculates the laminar, transition, and turbulent boundary-layer growth and separation point (if any) on the inlet surface. Lewis VISCUS[8] is a modified version of the Herring and Mellor program,[9] which calculates the laminar, transition, and turbulent boundary-layer development flow. The turbulence model and the boundary-layer transition criteria employed in the numerical solution are briefly described as follows.

Among all of the differential methods for the calculation of turbulent boundary layer, three of the so-called mean-flow methods[10] have been well explored for a wide range of turbulent shear flow; namely, the Cebeci-Smith (CS), Mellor-Herring (MH), and Patankar-Spalding (NP) methods. The CS and MH methods use the eddy viscosity approach and the NP method uses the mixing length approach to overcome the

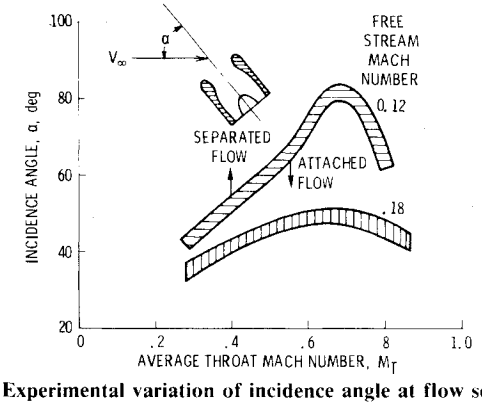

Fig. 2 Experimental variation of incidence angle at flow separation with average throat Mach number.

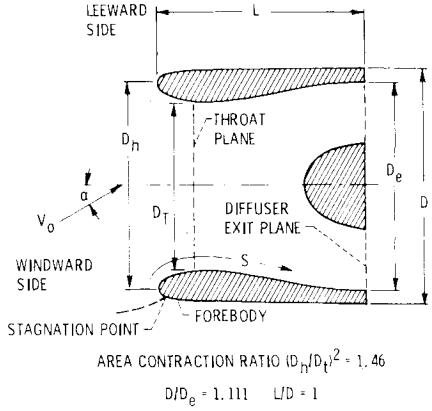

Fig. 1 Inlet geometry.

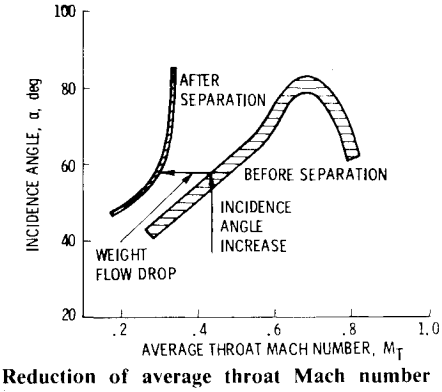

Fig. 3 Reduction of average throat Mach number due to flow separation (experimental data obtained by increasing incidence angle to point of flow separation) $M_0 = 0.12$.

turbulent closure problems. All three treat the boundary layer as a composite layer characterized by inner and outer regions and use separate semiempirical expressions for eddy viscosity ϵ_m or the turbulence length scale l in the two regions. Mellor and Herring[11] assume that in the inner region of an incompressible two dimensional (or axisymmetrical) flow with no heat transfer, the eddy viscosity is

$$(\epsilon_m)_i = \frac{x^4 \nu}{x^3 + (6.9)^3}$$

where

$$x = \frac{(ky)^2}{\nu}\frac{\partial u}{\partial y} \qquad (k = 0.41)$$

The eddy viscosity ϵ_m is defined in the following Reynolds stress tensor as

$$R_{ij} = \overline{u_i' u_j'} = \frac{1}{3} q^2 \delta_{ij} - \epsilon_m \left(\frac{\partial \bar{u}_i}{\partial x_j} + \frac{\partial \bar{u}_j}{\partial x_i} \right)$$

where $q^2/2$ represents the kinetic energy of turbulence. In the outer region Mellor and Herring assume the eddy viscosity

$$(\epsilon_m)_0 = 0.016 U_e \delta_k^*$$

where the kinematic displacement thickness is given by

$$\delta_k^* = \int_0^\infty \left[1 - \left(\frac{u}{U_e} \right) \right] \mathrm{d}y$$

An extension of the MH method to handle compressible flows is done by assuming that the same values of the three empirical constants which appeared in the eddy viscosity functions, can be used in the compressible flow as well. Furthermore, by assuming constant turbulent and molecular Prandtl numbers, the same eddy viscosity functions are used in the energy equation, so that compressible boundary layers with heat transfer can be calculated. Details of this extension along with the corresponding numerical schemes may be found in Mellor and Herring's report.[12]

For comparison, another program, which is based on the Cebeci-Smith method, is used in replacing the VISCUS program in some of the boundary-layer calculations. No significant discrepancy between the MH and CS methods has been found, even in the critical separation calculations. The transition region is defined as the region between the critical point, where small disturbances in the flow cease to be damped out and begin to grow and spread, and the transition point where complete turbulent flow starts in the boundary-layer. The critical point is determined by the comparison between the kinematic displacement thickness Reynolds number and the theoretical critical Reynolds number at each calculating station. When the actual Reynolds number (RDT) exceeds the theoretical value, the critical point (RC) has been reached. Effects of compressibility in this program are correlated through the use of the kinematic displacement thickness Reynolds number

$$R_{\delta_k^*} = U_e \delta_k^* / \nu_w$$

which contains the wall values of the kinematic viscosity. The effects of pressure gradient in compressible boundary layers with pressure gradients and transpiration are obtained from a correlation presented in Fig. 17.22 of Schlichting.[13]

Once the critical point has been located, turbulance effect starts to appear in the calculation and the next step is to search for the transition point. The rapidity of passage from critical point to transition point is expressed as the difference between momentum thickness Reynolds numbers (RMT) at these two points, i.e.,

$$\Delta R_\theta = \left(\frac{U_e \theta}{\nu_w} \right)_{\mathrm{tr}} - \left(\frac{U_e \theta}{\nu_w} \right)_{\mathrm{cr}} = (\mathrm{RMT})_{\mathrm{tr}} - (\mathrm{RMT})_{\mathrm{cr}}$$

$$= (R_\theta)_{\mathrm{tr}} - (R_\theta)_{\mathrm{cr}}$$

where the θ is the momentum thickness.

This quantity has been correlated as a function of pressure gradient by Granville (Fig. 17.11 of Schlichting[13]). Again the program will calculate the local value of the momentum thickness at wall for each station and compute the local value of $\bar{K}$, the mean Pohlhausen parameter, which is defined by

$$\bar{K} = \frac{1}{x_{\mathrm{tr}} - x_{\mathrm{cr}}} \int_{x_{\mathrm{cr}}}^{x_{\mathrm{tr}}} \frac{\theta^2}{\nu} \frac{\mathrm{d}U_e}{\mathrm{d}x} \mathrm{d}x$$

where x_{tr} is the local point of the calculation.

The computer will read the corresponding value of ΔR_θ, then the local transition momentum thickness Reynolds number $(\mathrm{RMT})_{\mathrm{tr}}$ may be calculated by the equation for ΔR_θ given earlier. When the Reynolds number based on local momentum thickness RMTW exceeds this transition Reynolds number $(\mathrm{RMT})_{\mathrm{tr}}$, then the transition point has been located.

Longitudinal wall curvature and wall roughness are introduced in the program through the use of influence coefficients. The influence coefficients for longitudinal curvature, $F_c(\theta/c_w)$ are derived from Liepmann's data as given in Fig. 17.38 of Schlichting,[13] by normalizing with zero curvature value of Reynolds number. Similarly, the roughness coefficient $F_R(S_w/\delta^* k)$ is derived from zero pressure gradient measurements by Feindt (Fig. 17.44 of Schlichting[13]) in a convergent or divergent channel of circular cross section with a cylinder covered with sand placed axially therein. It is observed that the sand roughness has no influence on transition when $U_e K_s/\nu < 120$, where K_s is the sandgrain size. The program also contains the calculation of the effect of heat transfer on transition based on Lees criterion.[9] However, this effect is not included in the present investigation and, hence, the discussion of it is omitted. The effect of turbulence intensity based on Granville's data (Fig. 16.21 of Schlichting[13]) is introduced to modify the transition Reynolds number by an influence coefficient $F_T(q^2/U_e^2)$ where q^2/U_∞^2 is the freestream turbulence level and can be specified in the input list. Finally, the complete expression for the transition Reynolds number becomes

$$R_{\theta_{\mathrm{tr}}} = [R_{\theta_{\mathrm{cr}}} + \Delta R_\theta F_T] F_R F_S$$

where the transition point is that at which the momentum thickness Reynolds number of boundary layer R_θ becomes greater than the local value of $R_{\theta_{\mathrm{tr}}}$.

The basic numerical scheme of the VISCUS program can be described as an implicit, Crank-Nicholson scheme resulting at each station in an ordinary differential equation which is solved according to a Runge-Kutta method adapted to the laminar and turbulent boundary-layer equations. Details of this numerical scheme can be found in Ref. 9.

The boundary-layer program calculates boundary-layer velocity profiles displacement thickness δ^*, skin friction coefficient C_f, etc., at each station. The boundary-layer calculation proceeds from laminar flow (at the stagnation point) through transition into turbulent flow. Transition is predicted based on the empirical correlations of Ref. 6. Flow separation is indicated by zero wall shear stress, i.e., when the local skin friction coefficient is zero.

The boundary-layer calculations are based on the assumption that the flow is axisymmetric. Thus, any secondary flow due to the inlet being at nonzero angle of attack is neglected.

There are additional shortcomings of the boundary-layer calculation. Many inlets of current interest, including the QCSEE inlet investigated herein, contain regions of local supersonic flow. Thus, there is the possibility of shock/boundary-layer interaction, which the present analysis does not account for. Also, the transition model does not account for the separation bubbles that are evident in some of the inlet surface static pressure distributions. In spite of these shortcomings, generally good agreement has been obtained with experimental data.[14]

Results and Discussion

Theoretical results are presented for the inlet of Fig. 1 at two values of freestream Mach number and a range of values of throat Mach number and inlet incidence angle. At both freestream Mach numbers, predicted and experimental separation bounds are compared. For one typical case, the boundary-layer development is given in some detail. Finally, the effects of surface roughness and model scale are illustrated.

Freestream Mach Number 0.12

The effect of incidence angle on two important flow parameters on the inlet windward internal surface is shown in Fig. 4 as a function of the surface distance from the inlet highlight for a throat Mach number of 0.59. Three values of incidence angle were selected to illustrate attached flow (56 deg), diffuser separation (64 deg), and lip separation (92 deg).

Figure 4a shows the local surface Mach number distribution from the stagnation point ($M=0$) to the diffuser exit ($S/D_e \approx 1.0$). Note that increasing the incidence angle produces two effects unfavorable to maintaining attached flow: 1) it increases the peak Mach number near the highlight ($S/D_e=0$) and, consequently, the diffusion required to the diffuser exit; and 2) it moves the stagnation point ($M=0$) further around on the outside of the inlet (increasing negative values of S/D_e), thus increasing the boundary-layer buildup ahead of the peak Mach number.

The corresponding local skin friction coefficient distributions are shown in Fig. 4b. The criterion for boundary-layer separation is that the skin friction coefficient C_f goes to zero. Separation onset is defined to occur when $C_f=0$ and $dC_f/ds=0$ as illustrated in the figure. It is the "separation onset" that is plotted in the subsequent figures. Its value is usually estimated from calculations that fall on both sides of the onset. It can be seen from Fig. 4b that for $\alpha=56$ deg, the flow does not separate, but that two areas for potential separation exist. They are the minimum C_f points, one in the diffuser, $S/D_e=0.6$, indicating diffuser separation at this flow condition. A further increase in α to 92 deg causes C_f to go to zero on the lip, indicating lip separation. Note that diffuser separation is in the fully turbulent region and lip separation is at the beginning of the transition region and is essentially laminar separation.

The calculations that produced Fig. 4 can be repeated at several values of average throat Mach number M_T and a range of values of incidence angle α to determine separation onset incidence angle. The results can then be used to generate the separation onset curves shown in Fig. 5. The flow is attached below the curves and separated above the curves. There are two theoretical separation onset curves in the figure: one for diffuser separation and the other for lip separation. The experimental separation onset data are also shown on the figure. In all cases when the experimental separation was observed, it was from the inlet lip. However, the instrumentation was not capable of telling if the separation had initiated in the diffuser and then propagated rapidly upstream to the lip. This possibility will be considered in more detail in the discussions of this and several following figures.

As was noted in the experimental results presented in Fig. 3, when separation occurs the weight flow (and thus M_T) drops. It is hypothesized that if separation starts in the diffuser, the weight flow decreases continuously with the upstream movement of the separation point. Now consider the theoretical diffuser separation onset curve. It has a maximum at an M_T of about 0.6. To the right of this maximum if separation occurs, the weight flow drops, moving the inlet operating point to the left into the attached-flow region. Thus, to the right of the maximum, diffuser separation is stable, that is, it does not propagate upstream to the lip. However, if the incidence angle is increased sufficiently, the theory predicts the onset of lip separation. The predicted lip separation agrees reasonably well with the experimentally observed separation, which is also from the lip.

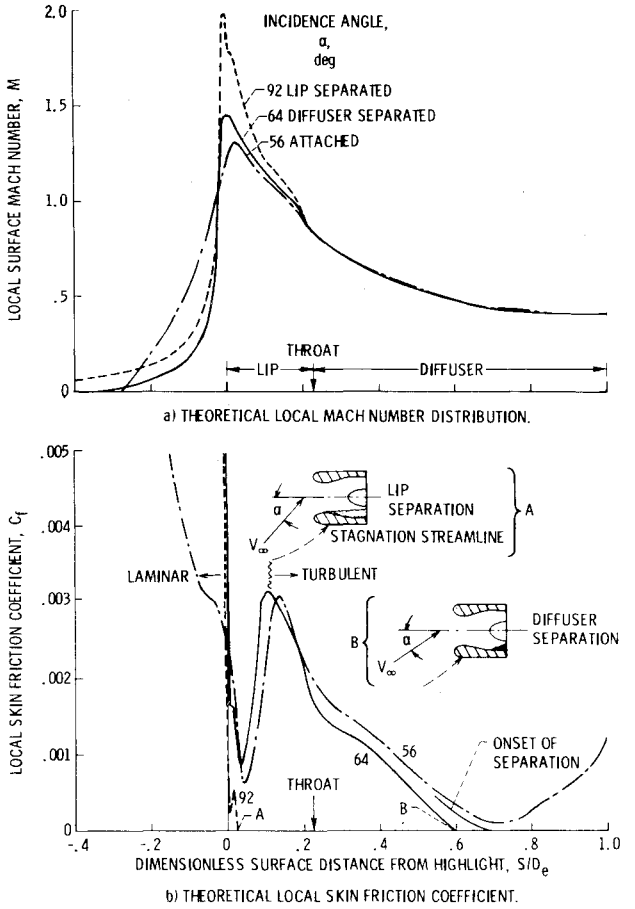

Fig. 4 Effect of incidence angle on flow separation, windward side of inlet, $M_0=0.12$, $M_T=0.59$.

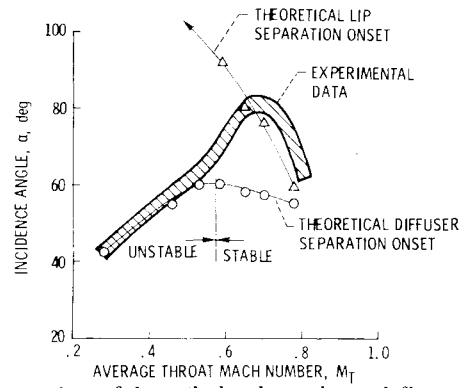

Fig. 5 Comparison of theoretical and experimental flow separation, $M_0=0.12$.

On the other hand, to the left of the maximum of the theoretical diffuser separation onset curve ($M_T < 0.6$), when diffuser separation occurs with the concomitant weight flow drop, the inlet operating point moves deeper into the separated region. Thus, to the left of the maximum diffuser separation is unstable, that is, it does propagate upstream to the lip. This type of separation is then observed in the experiment as occurring at the lip. With this interpretation, the theory and data agree.

Thus, for this inlet, the rules for interpreting analytical results for predicting the separation which will be observed experimentally as occurring from the inlet lip are 1) if the throat Mach number M_T is to the left of the maximum of the theoretical diffuser separation onset curve, the calculated diffuser separation angle is interpreted as the predicted lip separation angle; 2) if the throat Mach number is to the right of the maximum of the theoretical diffuser separation onset curve, the theoretical lip separation angle is also the predicted lip separation angle.

The stable and unstable regions of diffuser separation can also be illustrated theoretically. Figure 6a is a plot of local skin friction coefficient versus surface distance in the inlet for $\alpha = 56$ deg for several values of throat Mach number (weight flow) in the unstable region ($M_T < 0.6$). The reference curve is from a case of attached flow with $M_T = 0.59$. Reducing throat Mach number to 0.46 causes the flow to separate at an S/D_e of about 0.6. It is hypothesized that this separation causes a reduction in average throat Mach number. Reduction of throat Mach number (to 0.28, for example) moves the separation point further upstream, producing a greater extent of separated flow and reducing the weight flow still further. This process can continue until the separation reaches the lip.

On the other hand, Fig. 6b shows the effect of reducing the weight flow in the stable region. Starting with a throat Mach number M_T of 0.78, the flow is separated, which should reduce the average throat Mach number. Decreasing throat Mach number M_T to 0.70 causes the flow to become attached; reducing throat Mach number M_T further to 0.59 moves the flow even further from separation. Thus, a diffuser separation at these higher throat Mach numbers will not only not propagate upstream but the flow will tend to become attached when the weight flow drops due to diffuser separation.

The Mach number distributions for all the cases of Figs. 6a and 6b are shown on Fg. 6c. Note that there appears to be no obvious way of predicting whether a given case will separate or not by looking at the Mach number distribution. Even comparing a given Mach number distribution to one that is known to be attached or separated does not aid in prediction of the boundary-layer behavior.

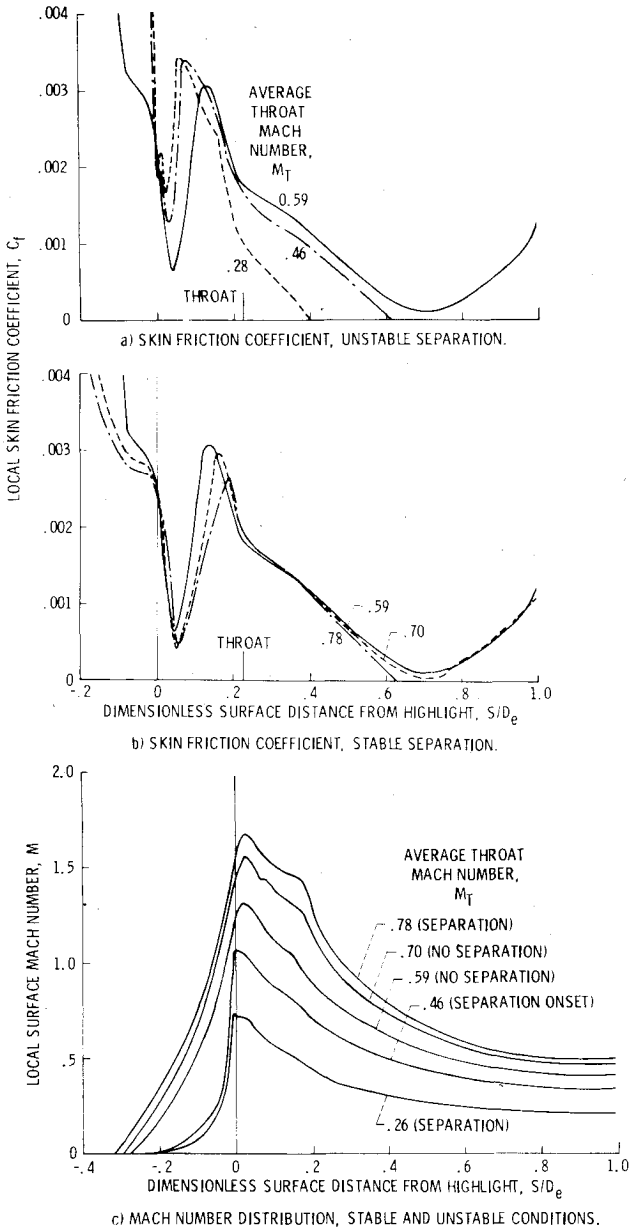

Fig. 6 Effect of average throat Mach number on location of separation, windward side, $M_0 = 0.12, \alpha = 56$ deg.

Freestream Mach Number of 0.18

Plots comparable to those of the previous section for a higher freestream Mach number of 0.18 (65m/s, 126 knots) are presented in Fig. 7. Figure 7a shows the effect on the local surface Mach number of varying the incidence angle at or near separation for a high throat Mach number of 0.73. The shapes of the Mach number distributions do not differ greatly from those of Fig. 4a; however, the incidence angle at which a given peak Mach number occurs is lower for the higher

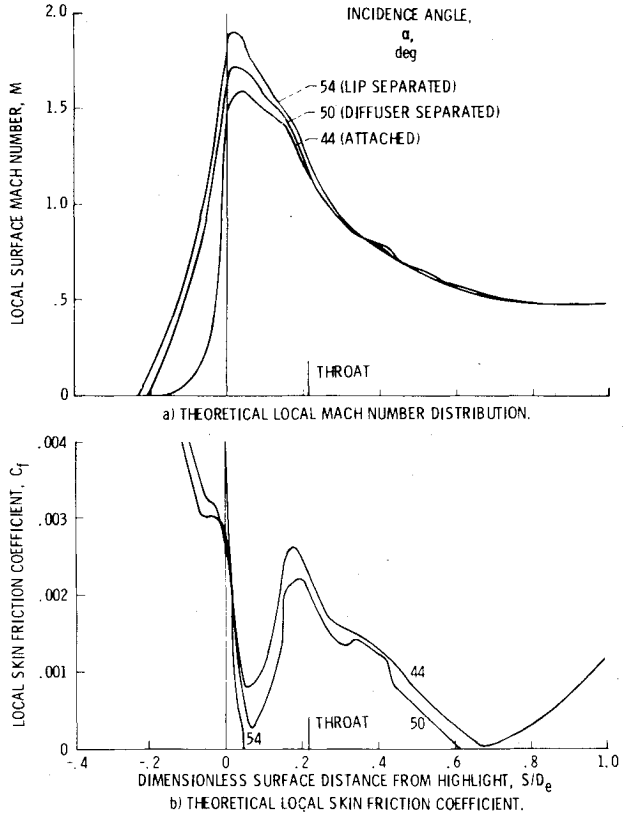

Fig. 7 Effect of incidence angle on flow separation, windward side, $M_0 = 0.18$, $M_T = 0.73$.

freestream Mach number case. Also, the angles at which diffuser and lip separation occur are lower here than for the $M_0 = 0.12$ case of Fig. 4a. The skin friction coefficient distributions are shown on Fig. 7b for the corresponding Mach number distributions of Fig. 7a. As before, this plot shows the location of the predicted separation point for each value of α: no separation at $\alpha = 44$ deg, diffuser separation at 50 deg, and lip separation at 54 deg.

Similarly, separation angles were found for other values of M_T, and the resulting separation onset curves are shown in Fig. 8 along with the experimental data for $M_0 = 0.18$. Once again, as in Fig. 5, the theoretical diffuser separation curve agrees with the experimental curve (where separation is observed to occur from the lip) to the left of the probable diffuser separation curve peak. To the right of this peak, there is little difference between the predicted lip and diffuser separation onset curves, and both are in reasonable agreement with the experimental data. Thus, the same interpretation of the theoretical results used to predict the observed experimental separation bounds at $M_0 = 0.12$, (Fig. 5) also applies here for $M_0 = 0.18$.

The effect of average throat Mach number on local flow conditions at $\alpha = 44$ deg is shown in Fig. 9. The local Mach number distributions (Fig. 9a) indicate, as before, that there is no obvious way of predicting from the Mach number distribution alone whether the inlet will separate or not. The corresponding skin friction distributions are shown in Fig. 9b, and again show the separation point moving upstream as the throat Mach number (weight flow rate) is decreased.

Boundary-Layer Details

Figure 10 shows the local skin friction coefficient and shape factor dstributions and also boundary-layer profile shapes and thickness at selected locations for a typical attached-flow case. The Mach number distributions corresponding to this case ($M_T = 0.80, M_0 = 0.18, \alpha = 44$ deg) are given on Fig. 9a). For comparision with the values of shape factors shown, the values for a flat plate are 2.6 for a laminar boundary-layer and 1.3 for a turbulent boundary-layer.

Upstream of the highlight ($S/D_e < 0$) the boundary-layer is thin and laminar, and the shape factor and velocity profile shown are representative of laminar flow. At the start of the transition region, there is a sharp increase in shape factor corresponding to a sharp drop in local skin friction coefficient and increase in the Mach number (Fig. 9a), i.e., in a very favorable pressure gradient. The shape factor reaches a peak value of 4.4 approximately where the skin friction reaches a minimum, both indications of a tendency to separation. Correspondingly, it can be judged from the shape of the dimensionless boundary-layer profile that the velocity gradient at the wall $d(u/U_0)/d(y/\delta)$ has decreased; a value of zero would, of course, indicate separation.

In the transition region as the boundary-layer becomes fully turbulent, the shape factor decreased rapidly, the skin friction coefficient increases, and the boundary-layer thickness δ/D_e continues to increase. The profile is fuller, $d(u/U_0)/d(y/\delta)$ has increased, so the boundary-layer has moved away from separation.

Midway down the diffuser, $S/D_0 \approx 0.7$, the turbulent boundary-layer parameters all show a tendency to separation; namely an increasing shape factor, a skin friction coefficient approaching zero, and a retarded boundary-layer profile. Toward the end of the diffuser the boundary-layer recovers a healthier set of characteristics.

Figure 10 has illustrated some of the details in the boundary layer typical of those for all of the preceding results. For all those cases, the surface was assumed to be smooth and the scale corresponds to a diffuser exit diameter D_e of 30.6 cm (12 in.). The following sections discuss the effect of surface roughness and scale.

Effect of Surface Roughness

The boundary-layer program accounts for the surface roughness through the input of the Nikuradse sand roughness.[15] To investigate this effect on the boundary-layer development, several values of Nikuradse sand roughness were considered. Although the program can handle roughness varying over the surface, for this study the roughness was constant over the entire surface for each case. Figure 11 shows the skin friction coefficent distribution for several values of roughness from zero (smooth wall) to 0.013 cm (0.005 in.). The inlet operating conditions ($M_T = 0.73, M_0 = 0.18$, $\alpha = 44$ deg) were chosen so that the smooth-wall case was very close to diffuser separation. It can be seen from the figure that a roughness of 0.0025 cm (0.001 in.) decreases the tendency toward separation on the lip as can be judged by the increase in the minimum local skin friction coefficient, but causes the flow to separate in the diffuser. Further increases in roughness appear to eliminate the laminar run, and move the turbulent separation point further upstream until, at a roughness of 0.013 cm (0.005 in.), the turbulent separation is almost on the lip.

A small extent of roughness near the highlight may be beneficial in reducing the tendency to laminar lip separation

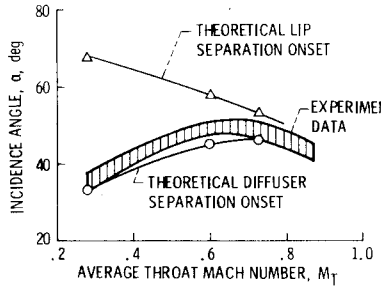

Fig. 8 Comparison of theoretical and experimental flow separation, $M_0 = 0.18$.

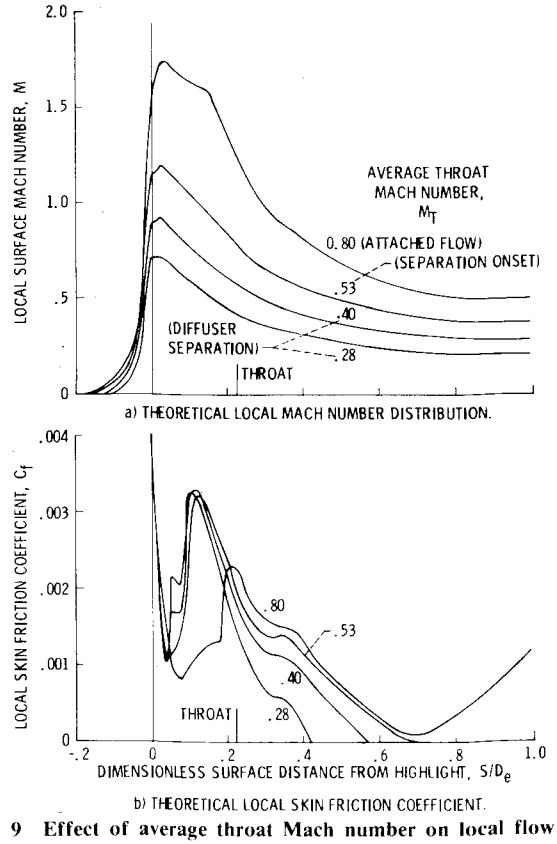

Fig. 9 Effect of average throat Mach number on local flow conditions, windward side, $M_0 = 0.18$, $\alpha = 44$ deg.

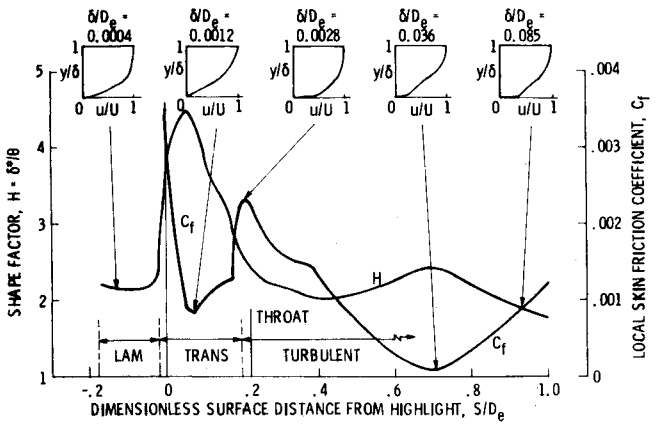

Fig. 10 Boundary-layer details, windward side, $M_0 = 0.18, \alpha = 44$ deg $M_T = 0.80$.

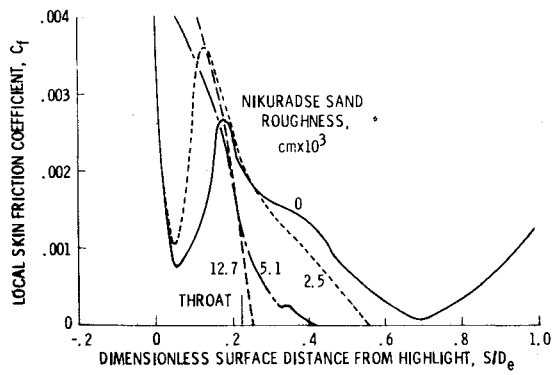

Fig. 11 Effect of surface roughness on separation, windward side, $M_0 = 0.18$, $\alpha = 44$ deg, $M_T = 0.73$

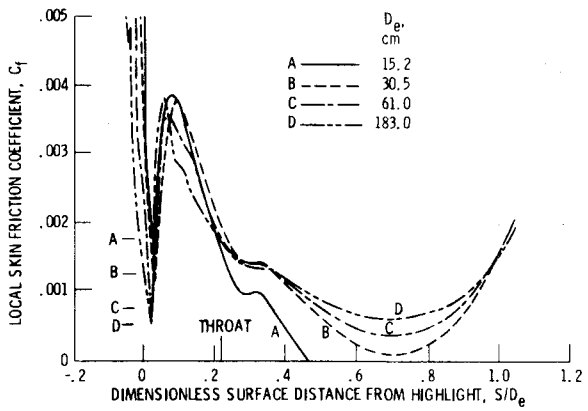

Fig. 12 Effect of scale on skin friction coefficient, windward side of inlet, $M_\infty = 0.13, \alpha = 41$ deg, $M_T = 0.28$.

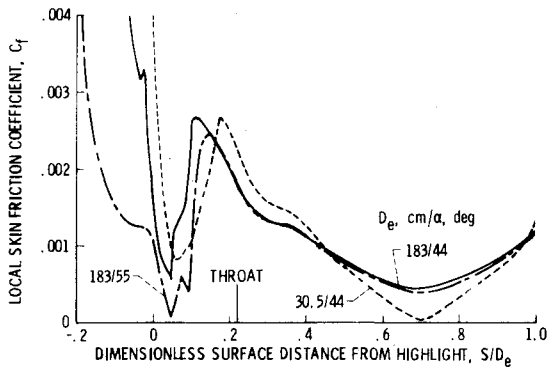

Fig. 13 Effect of scale and incidence angle on skin friction coefficient, windward side, $M_0 = 0.18$, $M_T = 0.73$.

with less adverse effect on the diffuser separation. This needs further study.

Effect of Scale

One of the goals of both wind-tunnel model tests and theoretical calculations is to be able to predict the boundary-layer behavior of full-scale inlets. A step toward this goal is the use of the present program to investigate the effects on the boundary-layer of changing the scale of the inlet of Fig. 1. Some data from this investigation are shown in Fig. 12 in the form of skin friction coefficient distributions. The flow conditions are such that the 30.5-cm base inlet is close to diffuser separation. If the scale is cut in half ($D_e = 15.2$ cm) the flow separates in the diffuser. As the scale is increased through $D_e = 61.0$ cm on up to full scale (183.0 cm), the flow becomes less likely to separate in the diffuser.

Note that the minimum C_f in the laminar region near the highlight decreases as scale increases, indicating that the lip is closer to laminar separation at the larger scale. This is because at the larger size, there is a longer laminar run with a resulting thicker laminar boundary-layer.

Further calculations can translate these kinds of results into the change in separation onset angle with scale. Results from preliminary calculations toward that end are shown in Fig. 13. Flow conditions are $M_0 = 0.18$ and $M_T = 0.73$; the base α is 44 deg. These conditions of scale model ($D_e = 30.5$ cm) are very close to separation in the diffuser; however, the full-size inlet ($D_e = 183$ cm) is a "safe" distance from diffuser separation. If α is increased to 55 deg for the full-size inlet, the diffuser boundary-layer characteristic is hardly different from that at 44 deg; however, the lip is now very close to separation. And, in fact, further calculations indicate that the lip separates at $\alpha = 55.5$ deg. Reference to Fig. 7b shows that the small-scale model also suffered lip separation for these flow conditions ($M_0 = 0.18, M_T = 0.73$) at $\alpha = 54$ deg, not greatly different from 55.5 deg. Thus, for this particular case it appears that increasing the scale can improve the diffuser performance significantly but not the lip performance.

Concluding Remarks

The Lewis subsonic inlet programs have been used to investigate the boundary-layer characteristics in an engine inlet. Comparison of calculated results with experimental data for this engine inlet indicates that, when interpreted properly, the theoretical results can be used to adequately predict inlet separation bounds. The interpretation rests in hypothesizing the existence of two types of diffuser separation, termed here stable and unstable. Unstable separation is defined to be diffuser separation that propagates upstream to the lip. An experiment is required to test this hypothesis. Also, the present approach needs to be applied to additional inlets to hopefully establish its generality.

The preliminary results presented on the effects of surface roughness and scale indicate that adding lip roughness may result in a more significant improvement in boundary-layer performance at larger scale than at small scale. A further investigation of the effects of roughness and scale is needed.

The analysis technique itself could be improved in several areas: 1) incorporate shock/boundary-layer interaction into the calculations, 2) provide the automatic sweep of incidence angle to determine separation onset, and 3) incorporate automatic geometry optimization techniques. These improvements should make the boundary-layer program a still more accurate and useful tool for subsonic inlet design and analysis.

References

[1] Stockman, N.O., "Potential and Viscous Flow in VTOL, STOL, or CTOL Propulsion System Inlets," AIAA Paper 75-1186, Anaheim, Calif., 1975.

[2] Albers, J.A. and Stockman, N.O., "Calculation Procedures for Potential and Viscous Flow Solutions for Engine Inlets," *Journal of Engineering for Power,* Vol. 97, Jan. 1975, pp. 1-10.

[3] Albers, J.A., Stockman, N.O., and Hirn, J.J., "Aerodynamic Analysis of Several High Throat Mach Number Inlets for the Quiet Clean Short-Haul Experimental Engine," NASA TMX-3183, 1975.

[4] Miller, B.A., Dastoli, B.J., and Wesoky, H.L., "Effect of Entry-Lip Design on Aerodynamics and Acoustics of High-Throat-Mach-Number Inlets for the Quiet, Clean, Short-Haul Experimental Engine," NASA TM X-3222, 1975.

[5] Stockman, N.O. and Button, S.L., "Computer Programs for Calculating Potential Flow in Propulsion System Inlet," NASA TMX-68278, 1973.

[6] Hess, J.L. and Smith, A.M.O., "Calculation of Potential Flow About Arbitrary Bodies," *Progress in Aeronautical Sciences,* Vol. 8, edited by D. Kuchemann, Pergamon Press, New York, 1967, pp. 1-138.

[7] Lieblein, S. and Stockman, N.O., "Compressibility Correction for Internal Flow Solution," *Journal of Aircraft,* Vol. 9, April 1972, pp. 312-313.

[8] Albers, J.A. and Gregg, J.L., "Computer Program to Calculate Laminar, Transition and Turbulent Boundary-Layers for Compressible Axisymmetric Flow," NASA TN D-7521, 1974.

[9] Herring, H.J. and Mellor, G.L., "Computer Program for Calculating Laminar and Turbulent Boundary Layer Development in Compressible Flow," NASA CR-2068, 1972.

[10] Cebeci, T. and Smith, A.M.O., *Analysis of Turbulent Boundary Layers,* Academic Press, New York, 1974.

[11] Mellor, G.L. and Herring, H.J., "Computation of Turbulent Boundary Layers," *AFOSR-IFP-Stanford Conference,* edited by S.J. Kline et al., Vol. 1, Stanford Press, Stanford, Calif. 1968, p. 331.

[12] Herring, H.J. and Mellor, G.L., "A Method of Calculating Compressible Turbulent Boundary Layers," NASA CR-1144, also N68-35096, 1968.

[13] Schlichting, H., *Boundary Layer Theory,* 6th Ed., translated by J. Kestin, McGraw-Hill, New York, 1968.

[14] Felderman, E.J. and Albers, J.A., "Comparison of Experimental and Theoretical Boundary-Layer Separation for Inlets at Incidence Angle at Low-Speed Conditions," NASA TM X-3194, 1975.

[15] Nikuradse, J., "Laws of Flow in Rough Pipes," NASA TM-1292, 1950.